IOP Publishing Physica Scripta
Phys. Scr. 95 (2020) 055217 (10pp) https://doi.org/10.1088/1402-4896/ab72c1

Impact of thermophoresis and brownian motion on non-Newtonian nanofluid flow with viscous dissipation near stagnation point

Kaleem Ashraf[1,3], **Imran Siddique**[1] **and Azad Hussain**[2]

[1] Department of Mathematics, University of Management and Technology, Lahore, Pakistan
[2] Department of Mathematics, University of Gujrat, Gujrat, Pakistan

E-mail: f2017265001@umt.edu.pk

Received 25 October 2019, revised 25 January 2020
Accepted for publication 4 February 2020
Published 3 March 2020

Abstract
In present manuscript, we have explored three dimensional non-Newtonian nanofluid flow with radiation impact considering dissipation in a vertical cylinder. The flow analysis is made in the existence of stagnation point. Radiative heat flux is estimated by Rosseland model. Thermophoresis and Brownian motion are the glamorous features for the delineation of nanofluids. Appropriate similarity transformations are applied to reduce the governing system of (PDE'S) together with boundary conditions into dimensionless form by taking boundary layer approximation. Arising coupled system of nonlinear (ODE'S) accompanied by boundary conditions are set about by powerful bvp4c method in Matlab software. Graphs and tables are drawn to present the influence of physical parameters. Skin friction and Nusselt number are contemplated for several parameters. Mounting the Eyring-Powel fluid parameter M_1 quickens the fluid velocity and enhance the temperature.

Keywords: dissipation effect, Rosseland model, vertical cylinder, eyring-powel fluid, bvp4c, stagnation point

(Some figures may appear in colour only in the online journal)

1. Introduction

Fluids with nano-size particles are called nanofluids. Nanoparticles accumulated in base fluids like oil and water leads to rise the heat transfer rate. Nanofluids play a significant role in heat exchanging industries to magnify the heat transfer. For the development of efficient heat transfer devices thermal conductivity plays an important role, but the regular fluids are poor heat transfer fluids like oil and water. To meet the worldwide competition in industries fluids with higher thermal conductivity are needed. Nanofluids have escalated thermal conductivity of fluids examined by Choi [1]. Practically, nanofluids are widely used to enhance the heat transfer rate in computer microchips, Bio medicine, nuclear reactor cooling and manufacturing [2–6]. Nadeem *et al* [7] analyzed a new category of nanofluids and concluded nanoparticles may be tabular or rod like. Nanoparticles of gold can be used as therapy for cancer treatment rather than drugs discovered by Jain *et al* [8]. Khan *et al* [9] examined stability of heat transfer and fluid flow of nanoparticles over a curved surface by dual nature solution. Many researchers have worked on nanufluids [10–14]. Sheikholeslami *et al* [15] analyzed the Lorentz force impact of heat transfer executing solidification in a porous medium. Mixed convective flow of Eyring-Powel nanofluid over a cone and plate is examined by Khan *et al* [16]. The movement of MHD micropolar nanfluid was numerically examined by Sadiq *et al* [17].

Many researchers are working on stagnation point flow now a days due to their vast applications in engineering and industries. Nadeem *et al* [18] analyzed the flow of compact

[3] Author to whom any correspondence should be addressed.

surface moving in the fluid. Rehman *et al* [19] studied stagnation point flow of second grade fluid over exponentially stretched sheet. Stagnation point flow by considering slip conditions for an electric conducting fluid is presented by Ramzan *et al* [20]. Malik *et al* [21] analyzed stagnation point flow of nanofluids stressed in a porous medium. Pal *et al* [22] presented the convective flow using heat generation and absorption for nanofluid over a stretched or shrinking sheet for a porous medium and concluded that the temperature of copper-water increases for large values of heat generation and absorption. Mehmood *et al* [23] examined radiating casson fluid over a stretched surface. Naseem *et al* [24] investigated third grade nanofluid by Cattaneo-Christove model over a riga plate. Ghadikolai *et al* [25] studied that the stagnation point flow occurs where the velocity of fluid is zero. MR Eid. [26] analyzed water-NPs flow in a porous medium over a stretching sheet considering stagnation-point with chemical reaction.

Non-Newtonian fluids has gained immense interest of researchers and engineers because of their extensive applications in industries and engineering. Blood, soaps, paints etc are non-Newtonian fluids. Physiological fluids are specified as non-Newtonian fluids with more difficulties on multiple stages analyzed by Abdelsalam *et al* [27]. Blood occupies many suspensions containing, electrolytes, gases, proteins, nutrients and leukocytes etc. The linear constitutive relations for shear stress and strain are not applicable to analyze non-Newtonian fluids due to non-linear relation between stress and strain. Several models have been developed to study these fluids, like Casson fluid model, Maxwell fluid and Eyring-Powel fluid. Many researchers analyzed mathematical modeling of these fluids [28–40]. Eyring and Powel firstly presented the Eyring-Powel fluid model in 1944. Eyring-Powel fluid model plays a vital rule in chemical engineering, controlling environmental pollution, formation and dispersion of fog etc. Nadeem *et al* [41] analyzed the Eyring-Powel nanofluid for stagnation point flow in the moving cylinder. MHD flow of Eyring-Powel fluid analyzed by Akbar *et al* [42] by applying implicit finite difference method and show that for large values of intensity resistance increases to flow.

In recent years, analysis of boundary layer flow over a cylinder has gained much interest of researchers due to vast applications. Production of fiber glass, chimney stacks, wire drawing are applications in this area [43]. Ellahi *et al* [44] examined MHD boundary layer flow under slip condition in a moving plate with entropy generation. Rizwan *et al* [45] analyzed boundary layer flow of nanoparticles under thermo-physical impact over a stretching surface. Recently Rehman *et al* [46] investigated the boundary layer flow of an Eyring-Powel fluid in a vertical cylinder considering the effect of heat transfer. MR Eid. [47] studied boundary-layer flow of two-phase model with heat generation and chemical reaction over an exponentially stretching sheet.

Literature shows boundary layer flow of Eyring-Powel nanofluid over a vertical cylinder considering variable properties is not studied yet. The aim of this study is to examine the radiative effect on Eyring-Powel nanofluid in a vertical cylinder considering boundary layer flow with heat transfer.

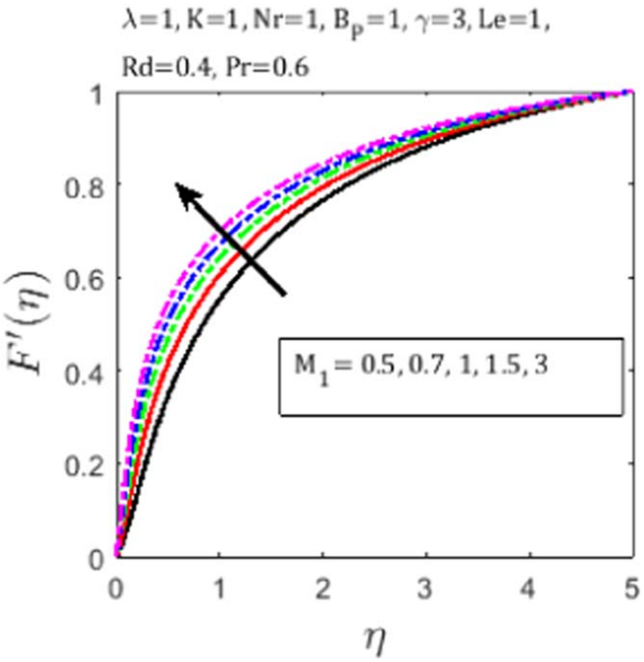

Figure 1. Influence of Fluid parameter M_1 on $F'(\eta)$.

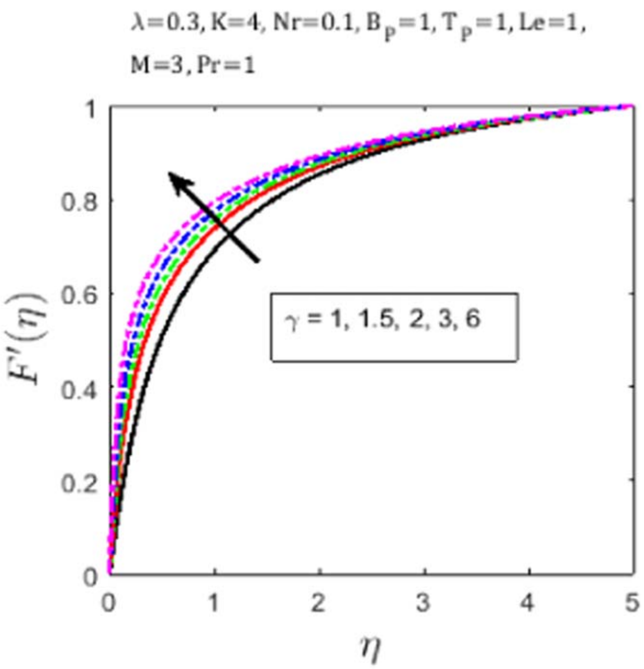

Figure 2. Influence of γ on $F'(\eta)$.

2. Mathematical formulation of problem

Consider stagnation point flow of an Eyring-Powel nanofluid through vertical slender cylinder of small radius a, considering dissipation effects. The coordinates $(x,\ r)$ are such that x is taken along the surface and r is in the radial direction. The velocity, temperature and concentration profiles are

$$V(x,\ r) = (w(x,\ r),\ 0,\ u(x,\ r)),$$
$$T = T(x,\ r), \quad \varphi = \varphi(x,\ r)$$

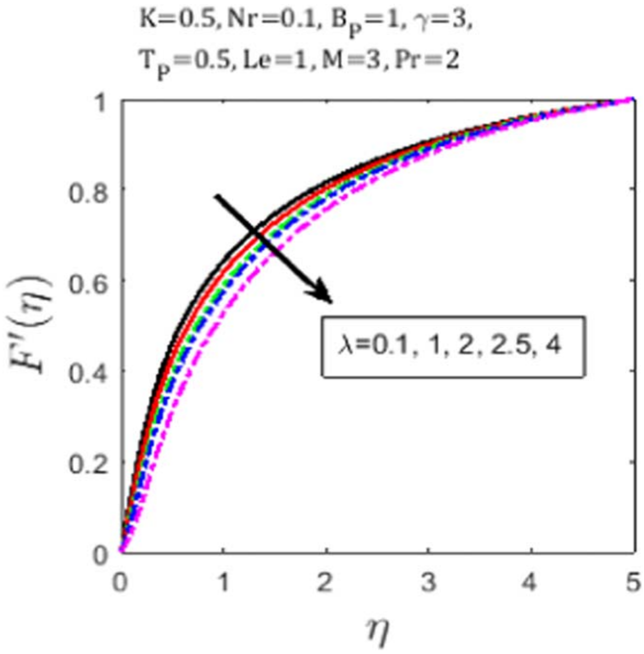

Figure 3. Influence of λ on $F'(\eta)$.

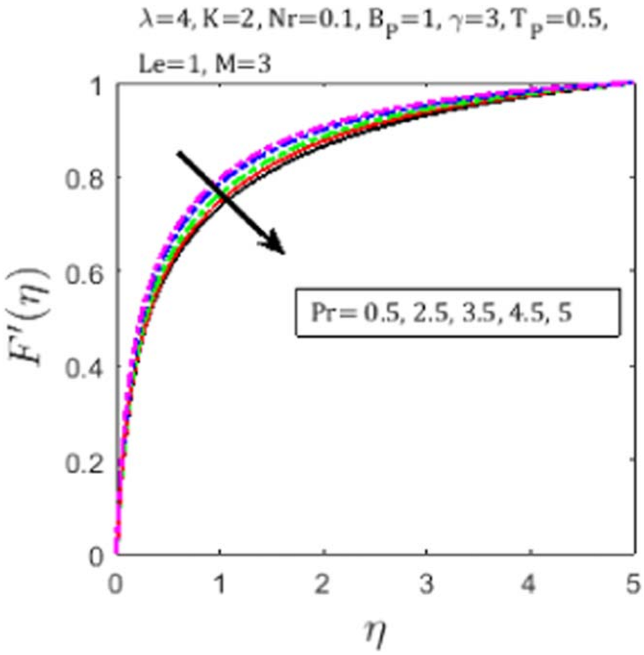

Figure 4. Influence of Pr on $F'(\eta)$.

Where $(w,\ u)$ denotes the velocity components. Boundary conditions corresponding to the given problem are

$$\text{at} \quad r = a, \quad u = 0, \quad T = T_w(x), \quad \varphi = \varphi_w(x). \tag{1}$$

$$\text{for} \quad r \to \infty, \quad u = U(x), \quad T \to T_\infty, \quad \varphi \to \varphi_\infty. \tag{2}$$

Where q_f is the radiative flux over surface of cylinder and T_∞ is the uniform ambient temperature. For the stimulated flow $T_w - T_\infty > 0$, also for the opposing flow $T_w - T_\infty < 0$. Stress tensor for the Eyring-Powel fluid is

$$A = -pI + \tau.$$

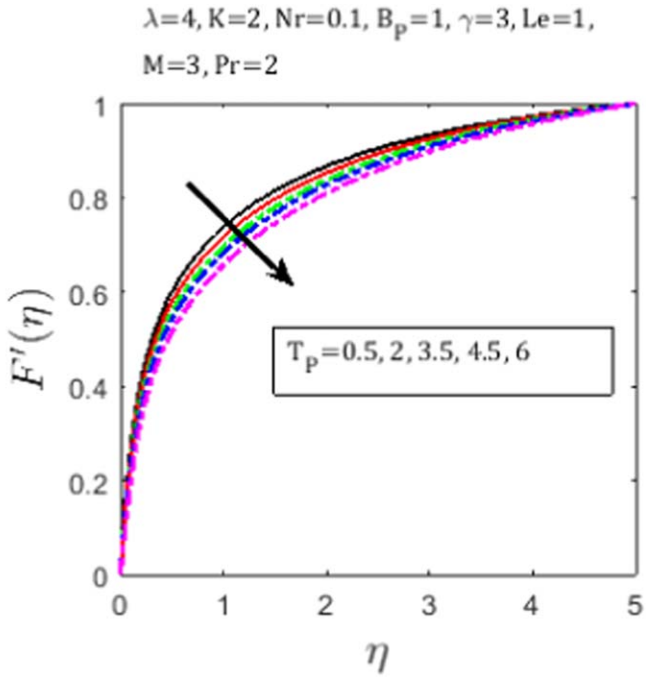

Figure 5. Influence of T_P on $F'(\eta)$.

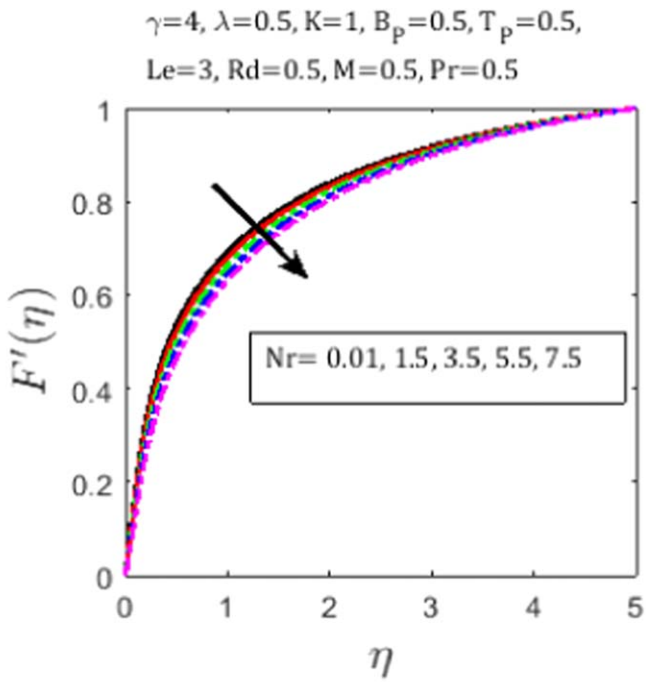

Figure 6. Influence of Nr on $F'(\eta)$.

Also shear stress component for Eyring-Powel fluid by [48] is

$$\tau_{i,j} = \mu_1 \frac{\partial w_i}{\partial u_j} + \frac{1}{\beta} \sinh^{-1}\left(\frac{1}{c}\frac{\partial w_i}{\partial u_j}\right). \tag{3}$$

Where μ_1 describes the viscosity, β and c are fluid parameters.

By considering dissipation effect, radiative effect and using boundary layer approximations momentum, energy and

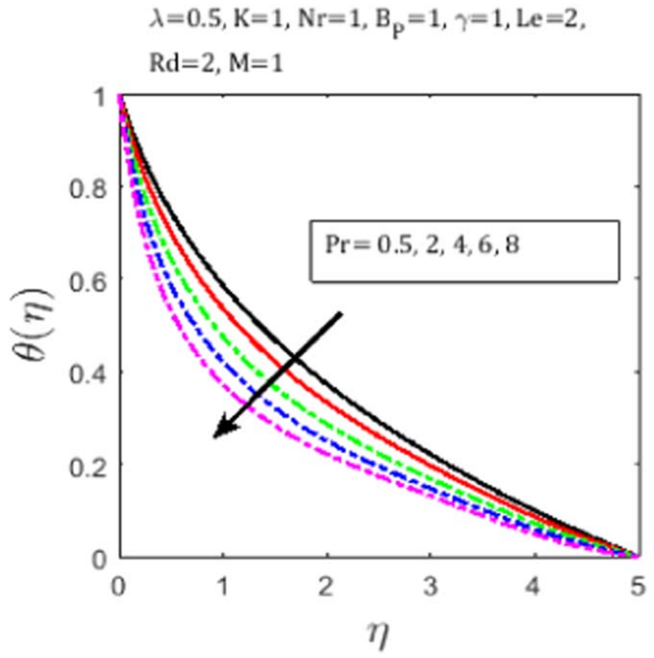

Figure 7. Influence of Pr on $\theta(\eta)$.

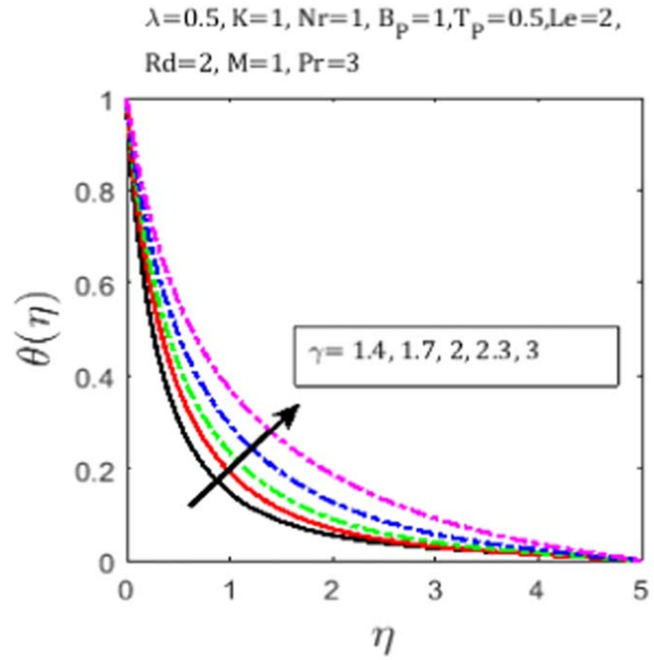

Figure 8. Influence of γ on $\theta(\eta)$.

concentration equations following [49] become

$$\frac{\partial(rw)}{\partial r} + \frac{\partial(ru)}{\partial x} = 0, \tag{4}$$

$$\begin{aligned} u\frac{\partial u}{\partial x} + w\frac{\partial u}{\partial r} = {} & U\frac{dU}{dx} + \upsilon(1 + M_1)\left(\frac{\partial^2 u}{\partial r^2} + \frac{1}{r}\frac{\partial u}{\partial r}\right) \\ & - \frac{2}{3\rho\beta c^3}\left[\frac{w^2}{r^2}\frac{\partial^2 u}{\partial r^2} + \frac{\partial u}{\partial r}\left(\frac{2}{r^2}w\frac{\partial w}{\partial r} - \frac{w}{r^3}\right.\right. \\ & + \frac{\partial u}{\partial x}\frac{\partial^2 u}{\partial x\partial r} - \frac{1}{r}w\frac{\partial^2 u}{\partial x\partial r} - \frac{\partial^2 w}{\partial r^2}\frac{\partial u}{\partial x} - \frac{\partial w}{\partial r}\frac{\partial^2 u}{\partial x\partial r} \\ & \left. - \frac{1}{r}\frac{\partial w}{\partial r}\frac{\partial u}{\partial x}\right) - \frac{\partial w}{\partial r}\frac{\partial^2 u}{\partial r^2}\frac{\partial u}{\partial x} + \beta^*(T - T_\infty) \\ & \left.\times (1 - \varphi_\infty)g\right] + \frac{(\rho_1^* - \rho_1)(\varphi_1 - \varphi_\infty)}{\rho_1}, \end{aligned} \tag{5}$$

$$\begin{aligned} w\frac{\partial T}{\partial r} + u\frac{\partial T}{\partial x} = {} & \alpha\left(\frac{\partial^2 T}{\partial r^2} + \frac{1}{r}\frac{\partial T}{\partial r}\right) + \frac{\upsilon}{c_p}(1 + M_1)\left(\frac{\partial u}{\partial r}\right)^2 \\ & - \frac{4\gamma M_1}{3c_p c^2}\left(\frac{\partial u}{\partial r}\right)^2\left[\frac{w^2}{r^2} - \frac{\partial w}{\partial r}\frac{\partial u}{\partial x}\right] + \rho_1^* c_p^* \\ & \times\left[D_B\left(\frac{\partial\varphi}{\partial r}\frac{\partial T}{\partial r} + \frac{\partial\varphi}{\partial x}\frac{\partial T}{\partial x}\right) + \frac{D_T}{T_\infty}\left(\frac{\partial^2 T}{\partial r^2} + \frac{\partial^2 T}{\partial x^2}\right)\right] \\ & - \frac{1}{r}\frac{\partial}{\partial r}[rq_f] = 0, \end{aligned} \tag{6}$$

$$\begin{aligned} w\frac{\partial\varphi}{\partial r} + u\frac{\partial\varphi}{\partial x} = {} & D_B\left(\frac{\partial^2\varphi}{\partial r^2} + \frac{1}{r}\frac{\partial\varphi}{\partial r}\right) + \frac{D_T}{T_\infty}\left(\frac{\partial^2 T}{\partial r^2}\right. \\ & \left. + \frac{\partial^2 T}{\partial x^2}\right). \end{aligned} \tag{7}$$

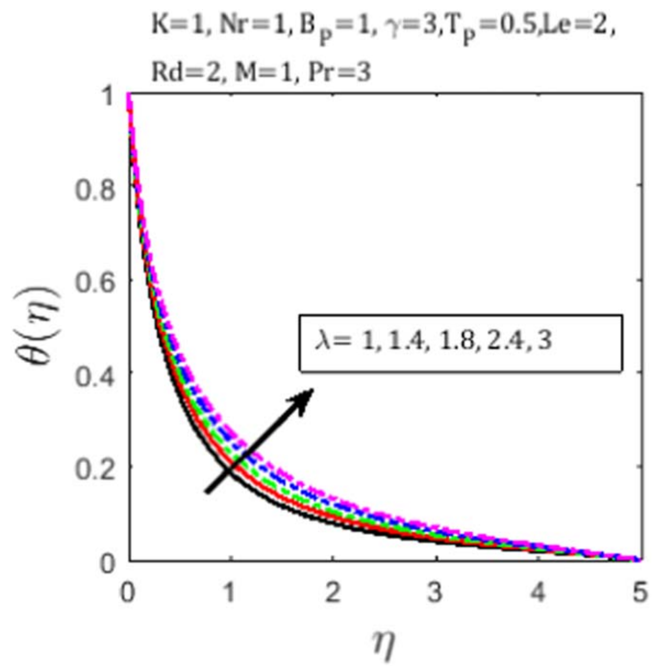

Figure 9. Influence of λ on $\theta(\eta)$.

Where the radiative heat flux q_f according to Rosseland model is given by,

$$q_f = \frac{-4\sigma_1^*}{3k_1^*}\frac{\partial T^4}{\partial r}.$$

By Taylor series T^4 can be written as,

$$T^4 = 4T_\infty^3 T - 3T_\infty^4.$$

So q_f becomes,

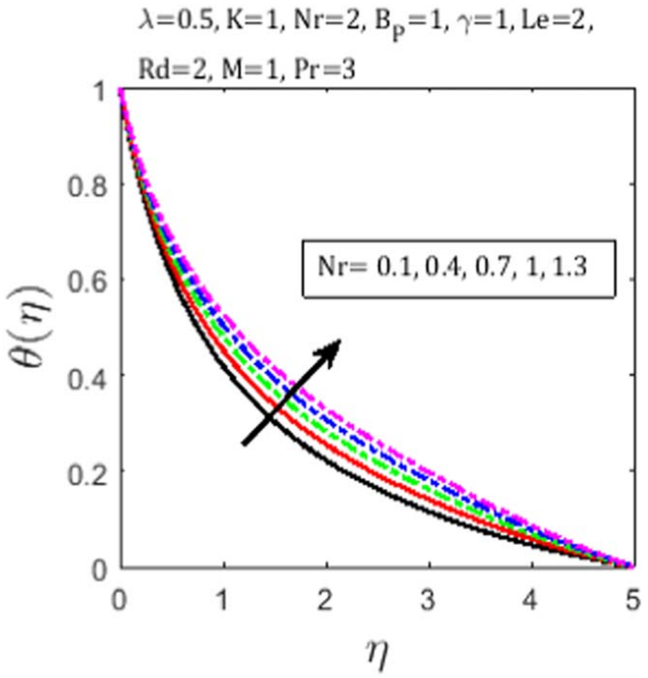

Figure 10. Influence of Nr on $\theta(\eta)$.

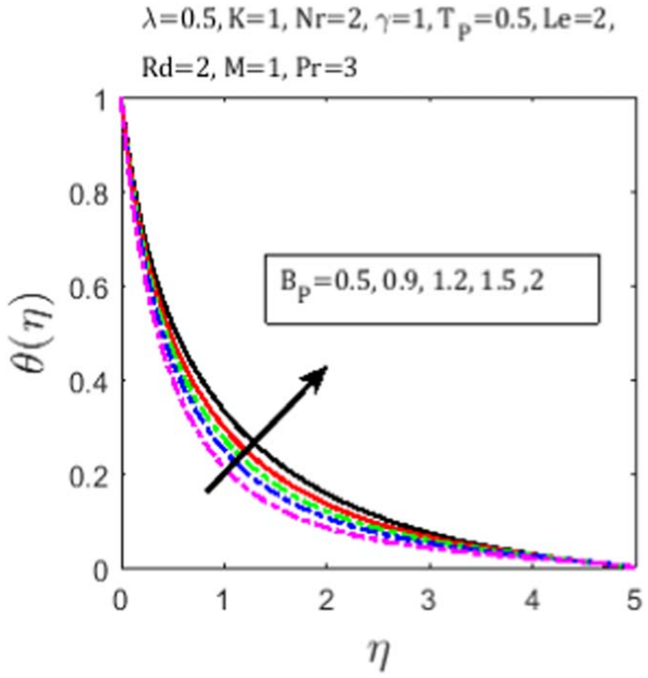

Figure 11. Influence of B_p on $\theta(\eta)$.

$$q_f = \frac{-16\sigma_1^*}{3k_1^*}\frac{\partial T}{\partial r}. \tag{8}$$

Here the velocity components w and u are taken along the x and z direction respectively, pressure is p, M_1 used for Eyring-Powel parameter, ρ denotes density of fluid, ρ_1 and ρ_1^* denotes the density of nanofluid inside and at the boundary, temperature is T, Concentration is φ, curvature is γ, g is gravitational acceleration, β & c denote material parameters, υ represents kinematic viscosity, thermal expansion coefficient is β^*, α denotes thermal diffusivity, c_p and c_p^* represent specific heat using constant pressure for the base fluid and nanofluid respectively, σ_1^* presents the Electric conductivity of fluid, k_1^* presents thermal conduction of fluid, velocity at the surface is taken as U_∞, free stream velocity is defined as

$$U = U_\infty\left(\frac{x}{l}\right).$$

3. Solution

By applying suitable similarity transformations [35]:

$$u = \frac{xU_\infty}{l}F'(\eta),\ w = \frac{-a}{r}\left(\frac{U_\infty}{l}\right)F(\eta) \tag{9}$$

$$\theta = \frac{T - T_\infty}{T_w - T_\infty},\ \eta = \frac{r^2 - a^2}{2a}\left(\frac{U_\infty}{\upsilon l}\right) \tag{10}$$

Transformation (9) and (10) convert the partial differential equations (4)–(7) into ordinary differential equation as follows

$$\begin{aligned} &-(1 + 2\gamma\eta)F''' + 2\gamma F'' + \frac{1}{1 + M_1}(1 + FF'' - F'^2) \\ &+ \frac{KM_1\gamma}{1 + M_1}\Bigg[(FF'F''' - F'^2F'') - \gamma(1 + 2\gamma\eta) \\ &\times (3FF''^2 + F'^2F''') - \frac{\gamma}{(1 + 2\gamma\eta)}(FF'F'' + F^2F''') \\ &+ \frac{2\gamma^2}{(1 + 2\gamma\eta)^2}F^2F''\Bigg] + \lambda\theta = 0, \end{aligned} \tag{11}$$

$$\begin{aligned} &(1 + Rd)(1 + 2\gamma\eta)\theta'' + 2(1 + Rd)\gamma\theta' + \Pr(F\theta' - F'\theta) \\ &+ (1 + 2\gamma\eta)B_P\theta'\psi' + T_P(1 + 2\gamma\eta)\theta'^2 + (1 + M_1) \\ &\times \Pr Ec(1 + 2\gamma\eta)F''^2 + 2KM_1\Pr Ec\Bigg[\gamma FF'F'' \\ &- (1 + 2\gamma\eta)F'^2F'' - \frac{\gamma^2}{(1 + 2\gamma\eta)}F'^2F''\Bigg] = 0, \end{aligned} \tag{12}$$

$$\begin{aligned} &(1 + 2\gamma\eta)\psi'' + 2\gamma\psi' + Le\Pr(F\psi' - F'\psi) + \frac{T_P}{B_P} \\ &\times ([(1 + 2\gamma\eta)\theta'' + 2\gamma\theta'] = 0. \end{aligned} \tag{13}$$

Where, $\gamma = \left(\frac{\upsilon l}{U_\infty a^2}\right)$ is curvature parameter, Buoyancy parameter $\lambda = \frac{g\beta^*\Delta Tx}{U_\infty^2}$, Eckert number $Ec = \frac{U_\infty^2}{c_p\Delta T}$, K and M_1 represent Eyring-Powel parameters $K = \frac{2U_\infty^2}{3c^2l^2}$, $M_1 = \frac{1}{\beta\mu c}$, $Nr = \frac{(\rho_1^* - \rho_1)(\phi_w - \phi_\infty)}{\rho_1\beta(T_w - T_\infty)(1 - \phi_\infty)}$ defines Buoyancy ratio, Brownian parameter for motion $B_P = \frac{\rho^* c_p^* D_B(\phi_1 - \phi_\infty)}{\rho c_p\alpha}$, thermal parameter

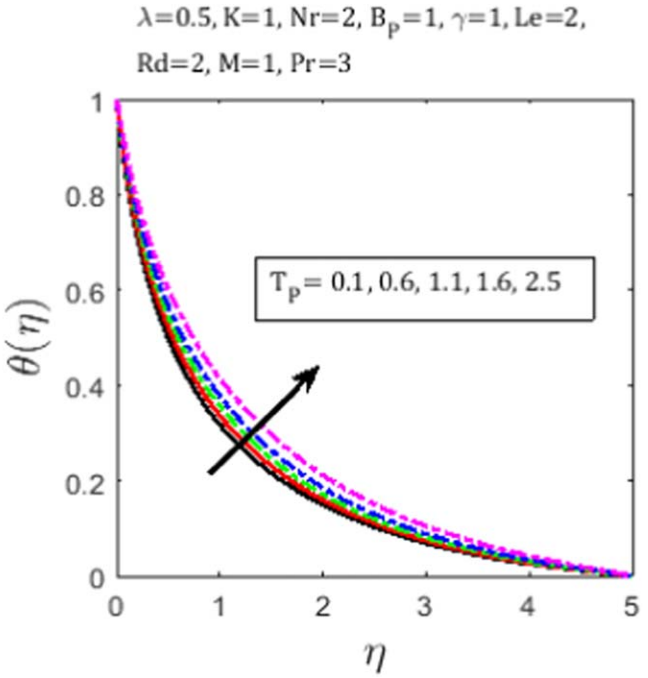

Figure 12. Influence of T_p on $\theta(\eta)$.

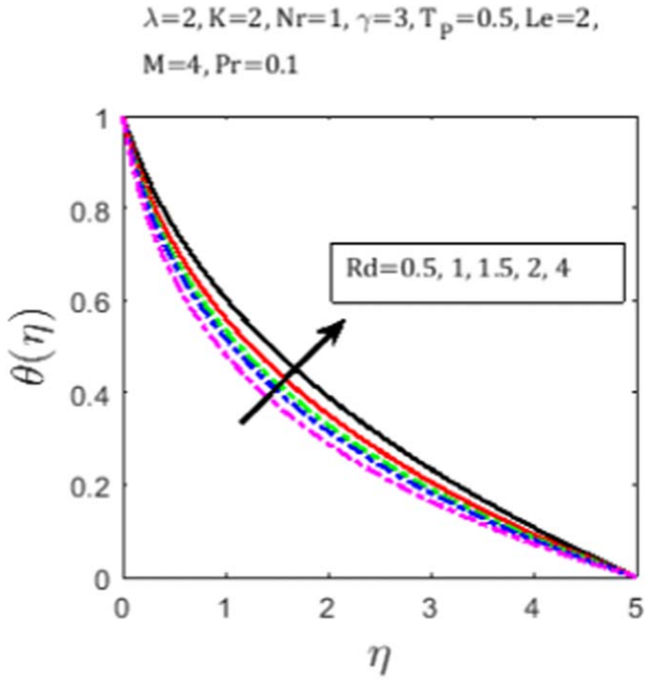

Figure 13. Influence of Rd on $\theta(\eta)$.

is $T_P = \frac{\rho^* c_p^* D_T(T_w - T_\infty)}{\rho c_p \alpha T_\infty}$, Lewis number is $Le = \frac{\alpha}{D_B}$ and Prandtl number is $\Pr = \frac{\upsilon}{\alpha}$.

Dimensionless boundary conditions are taken as

$$F(0) = 1,\ F'(0) = 0,\ F' \to 1,\ \text{ as } \eta \to \infty, \tag{14}$$

$$\theta(0) = 1,\ \theta \to 0, \text{ as } \eta \to \infty, \tag{15}$$

$$\psi(0) = 1,\ \psi \to 0,\ \text{ as } \eta \to \infty. \tag{16}$$

Stress over the surface of cylinder is τ_w, heat flux is q_w, N_u is Nusselt number and C_f is skin friction. These are fundamental physical quantities to be analyzed.

$$\frac{N_u}{\mathrm{Re}_x^{\frac{1}{2}}} = -\theta'(0),\ \tau_w = (\tau_{rx})_{r\to a},\ q_w = -k\left(\frac{\partial T}{\partial y}\right)_{y=0}, \tag{17}$$

$$\frac{1}{2} C_f \,\mathrm{Re}_x^{\frac{1}{2}} = (1 + M_1)F''(0) - \frac{1}{3} M_1 \lambda F''^3(0). \tag{18}$$

τ_{rx} is the component of stress in x-direction, Re_x is the Reynold number.

A powerful technique bvp4c is applied to find the solution of current problem and following assumptions are made

$$F(\eta) = y_1,\ F' = y_2,\ F'' = y_3,\ F''' = y'_3, \tag{19}$$

$$\theta(\eta) = y_4,\ \theta' = y_5,\ \theta'' = y'_5, \tag{20}$$

$$\psi(\eta) = y_6,\ \psi' = y_7,\ \psi'' = y'_7. \tag{21}$$

In view of equations (18)–(20) the resulting equations from (11) to (13) are as follow

$$\begin{aligned} y_3' = \Bigg[&2\gamma\, y_3 + \frac{1}{1 + M_1}\Bigg((1 + y_1 y_3 - y_2^2) - \frac{K M_1 \gamma}{(1 + M_1)} \\ &\times y_2^2 y_3 - \frac{3 K M_1 \gamma^2}{(1 + M_1)}(1 + 2\gamma\eta) y_1 y_3^2 \\ &- \frac{K M_1 \gamma^2}{(1 + 2\gamma\eta)(1 + M_1)} y_1 y_2 y_3 \\ &+ \frac{2 K M_1 \gamma^3}{(1 + M_1)(1 + 2\gamma\eta)^2} y_1^2 y_3 \\ &+ \lambda(1 - \phi_\infty)(y_4 + Nr y_6)\Bigg]\Bigg/ \\ &\times \Bigg[(1 + 2\gamma\eta) - \frac{K M_1 \gamma}{1 + M_1} y_1 y_2 + \frac{K M_1 \gamma^2}{1 + M_1} \\ &\times (1 + 2\gamma\eta) y_2^2 + \frac{K M_1 \gamma^2}{(1 + M_1)(1 + 2\gamma\eta)}\Bigg], \end{aligned} \tag{22}$$

$$\begin{aligned} y_5' = -\Bigg[&2\gamma(1 + Rd) y_5 + \Pr(y_1 y_5 - y_2 y_4) \\ &+ (1 + 2\gamma\eta) B_P y_5 y_7 + T_P (1 + 2\gamma\eta) y_5^2 \\ &- (1 + 2\gamma\eta) y_2^2 y_3 + (1 + M_1)\Pr Ec \\ &\times (1 + 2\gamma\eta) y_3^2 + 2 K M_1 \Pr Ec (\gamma y_1 y_2 y_3) \\ &- \frac{\gamma^2 y_2^2 y_3}{(1 + 2\gamma\eta)}\Bigg] / [(1 + Rd)(1 + 2\gamma\eta)]\,, \end{aligned} \tag{23}$$

$$\begin{aligned} y'_7 = -\Bigg[&2\gamma\, y_3 - Le\Pr(y_1 y_7 - y_2 y_6) - \frac{T_P}{B_P} \\ &\times ((1 + 2\gamma\eta) y_5' + 2\gamma\, y_5)\Bigg] / \,[(1 + 2\gamma\eta)]\,. \end{aligned} \tag{24}$$

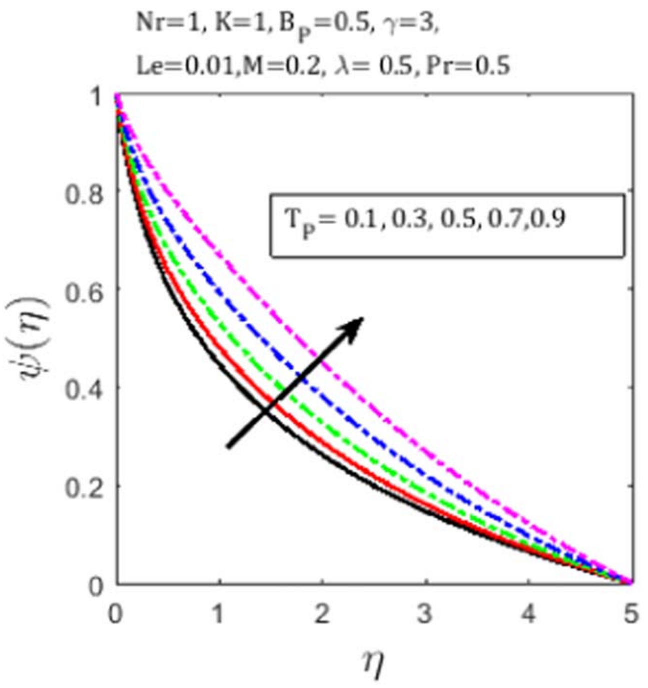

Figure 14. Influence of Tp on $\psi(\eta)$.

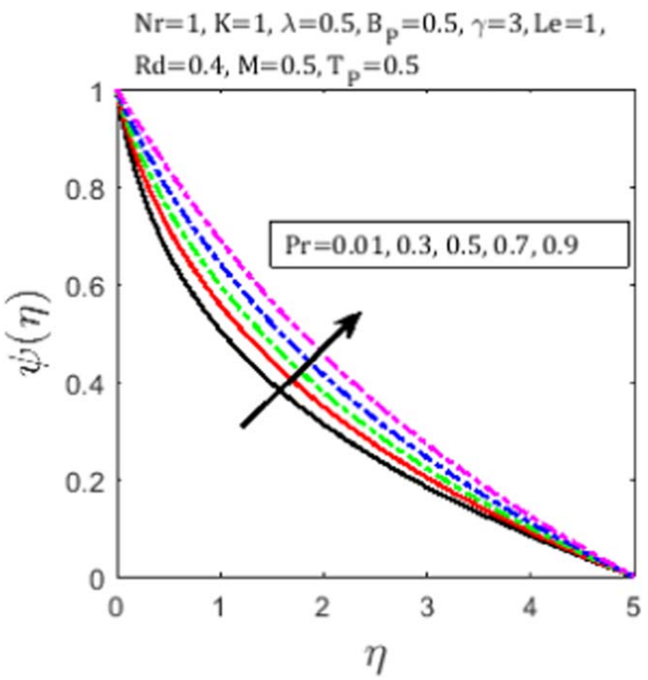

Figure 15. Influence of Pr on $\psi(\eta)$.

Numerical results for the solution are presented in the proceeding section.

4. Results and discussion

In current section, a short analysis of the influence of involved parameters is to be presented.

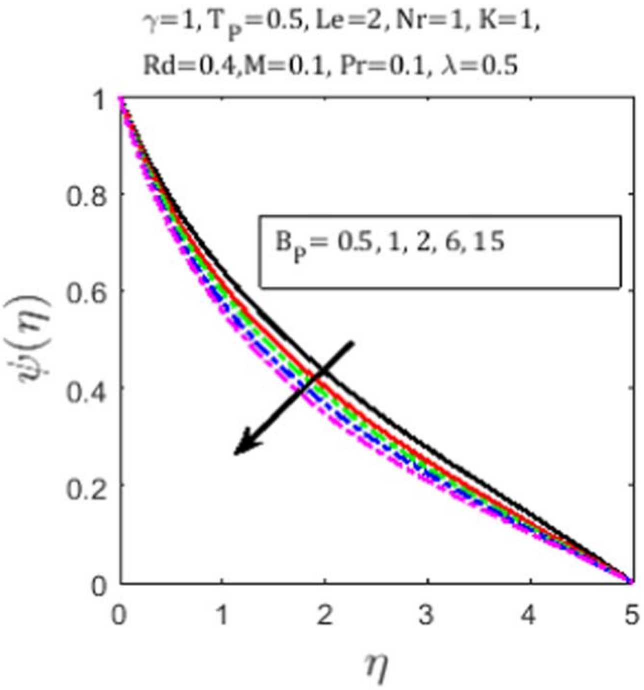

Figure 16. Influence of B_P on $\psi(\eta)$.

4.1. Velocity profile

Figures 1–6 show the influence of evolved parameters on fluid flow. Figure 1 presents the impact of Eyring-Powel parameter M_1 on the fluid velocity $F'(\eta)$. Fluid velocity increases as the Eyring-Powel parameter M_1 becomes higher. It is also noticed that with increase in fluid parameter M_1 fluid viscosity decreases, due to which the fluid velocity increases. Figure 2 depicts that with increase in curvature the fluid velocity becomes higher. With higher curvature, radius of cylinder decreases, resulting a less resistance to the fluid flow due to which $F'(\eta)$ increases. From figure 3 it is perceived that the increase in Buoyancy parameter λ enhance the nanoparticles mass density of the fluid and lessen the fluid velocity. Figure 4 exhibits with increase in Prandtl number boundary layer thickness decline, resulting the decrease in fluid velocity. The impact of nanoparticles parameters like thermophoresis and buoyancy ratio are presented in figures 5 and 6. It is noticeable that the fluid velocity shows decreasing behavior for both thermophoresis parameter T_P and buoyancy ratio Nr, which means velocity decreases with increase in ratio of nanoparticles mass density to that of fluid density.

4.2. Temperature profile

Figures 7–13 present the influence of some parameters over temperature field $\theta(\eta)$. Figure 7 depicts with increase in Prandtl number, thermal boundary layer thickness decline and temperature decreases. Increasing behavior of temperature profile is depicted in figure 8, with increase in curvature. Because increasing curvature minimize the rate of heat conduction due to which temperature rises. Temperature rises with increase in Buoyancy parameter shown in figure 9. Temperature escalates with increase in Nr presented in

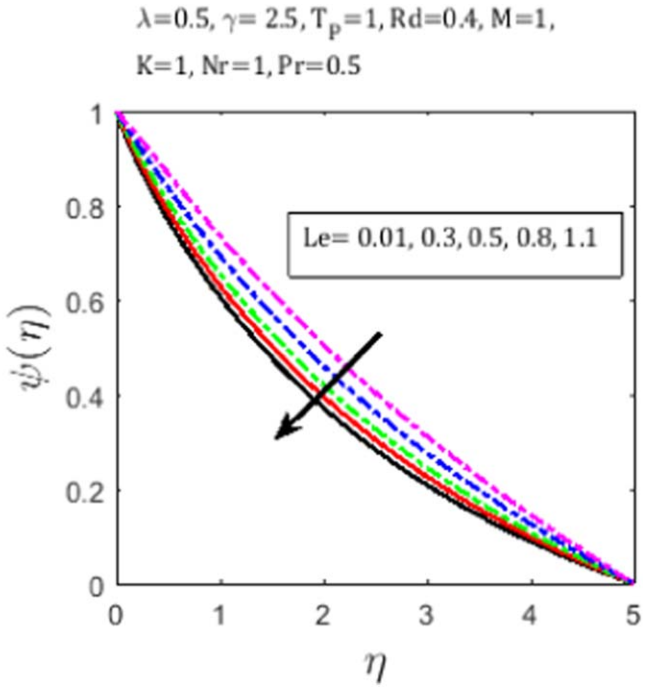

Figure 17. Influence of Le on $\psi(\eta)$.

Table 1. Skin friction for λ, K, N_r, γ, M.

λ	K	N_r	γ	M	$F''(0)$	C_f
0.1	0.1	0.1	0.1	0.1	−0.6836	−0.75089
0.2	—	—	—	—	−0.7419	−0.81328
0.3	—	—	—	—	−0.8001	−0.87498
0.1	0.2	—	—	—	−0.6833	−0.75056
—	0.3	—	—	—	−0.6834	−0.75067
—	0.4	—	—	—	−0.6835	−0.75078
—	0.1	0.5	—	—	−0.7042	−0.77345
—	—	0.6	—	—	−0.7094	−0.77914
—	—	0.7	—	—	−0.7145	−0.78473
—	—	0.1	0.8	—	−0.2975	−0.32716
—	—	—	0.9	—	−0.3184	−0.35013
—	—	—	1.0	—	−0.3423	−0.37639
—	—	—	0.1	1.1	−0.137	−0.28760
—	—	—	—	1.2	−0.1474	−0.32415
—	—	—	—	1.3	−0.5221	−1.19466

figure 10. With increase in Brownian motion parameter, nanoparticles collide with the base fluid molecules, which enhance the kinetic energy and rise the temperature exhibits in figure 11. In figure 12 variation of mophoresis parameter Tp is indicated. Thermophoresis is a process in which nanoparticles moves from higher temperature to lower, resulting the increase in temperature. Figure 13 indicates the impact of variation in heat flux parameter Rd on temperature profile. Practically, rise in the parameter Rd implies more heat is passed on to the nanofluid and enhances the temperature.

4.3. Concentration profile

Figure 14 depicts the concentration of nanoparticles increases with increase in Tp, because nanoparticles move away from

Table 2. Nusselt number for Ec, Pr, Rd.

Ec	Pr	Rd	$-\theta'(0)$
0.1	7	0.4	5.397
0.2	—	—	5.603
0.3	—	—	5.803
0.1	7	—	5.803
—	7.5	—	6.004
—	8	—	6.182
—	7	0.4	5.415
—	—	0.5	5.6
—	—	0.6	5.803

Table 3. Comparison of velocity profile with [49] for several values of $f(0) = b$ and γ, ignoring dissipation effect and radiative effect.

	$f''(0)$					
	[49]	Present	[49]	Present	[49]	Present
b/γ	0.5		1.0		1.5	
−1	0.9918	0.9918	1.1942	1.1942	1.3729	1.3729
0	1.4886	1.4886	1.7244	1.7244	1.7954	1.7954
1	2.0397	2.0397	2.1751	2.1751	2.2982	2.2982
2	2.7332	2.7332	2.8029	2.8029	2.8746	2.8746

the hot surface resulting enhancement in the concentration. Figure 15 concludes the Concentration profile decreases with increase in Prandtl number. Figure 16 is a good evidence that increase in Bp decreases the concentration. With increase in Brownian motion parameter nanoparticles collisions and random motion enhance, which decrease the concentration of fluid. Figure 17 indicates by increasing the Lewis number concentration decreases, because increasing Le mass diffusivity declines and reduces the concentration.

Table 1 is formed to check the influence of several parameters on skin friction. It shows that with increase in these parameters skin friction decreases. Table 2 is created to analyze the effects of Pr, Rd and Ec on Nusselt number. Table 3 illustrates the comparison between present and past study.

5. Conclusion

Stagnation point flow of three dimensional non-Newtonian fluid with variable temperature is examined. The following results are worth citing.

- The velocity profile escalates by rising the curvature γ and fluid parameter M, while temperature shows decreasing behavior.
- By enlarging the Prandtl number temperature profile decreases but rise with Brownian motion.
- Concentration of nanoparticles present decreasing behavior by increasing both the Brownian motion and Lewis number.
- Skin friction decreases by enhancing the fluid parameters K and M, but the Nusselt number rises with rise in Prandtl number.

ORCID iDs

Azad Hussain https://orcid.org/0000-0002-3100-582X

References

[1] Choi S U S 1998 *Nanofluid Technology: Current Status and Future Research* ANL/ET/CP-97466 Argonne National Lab. Argonne, IL, United States of America
[2] Ibrahim W, Shankar B and Nandeppanavar M M 2013 MHD stagnation point flow and heat transfer due to nanofluid towards stretching sheet *Int. J. Heat Mass Transfer* **56** 1–9
[3] Ellahi R 2013 The effects of MHD and temperature dependent viscosity on the flow of non-Newtonian nanofluid in a pipe: analytical solutions *Applied Mathematics and Modeling* **37** 1451–67
[4] Alrashed A A, Akbari O A, Heydari A, Toghraie D, Zarringhalam M, Shabani G A S and Goodarzi M 2018 The numerical modeling of water/FMWCNT nanofluid flow and heat transfer in a backward-facing contracting channel *Physica B* **537** 176–83
[5] Bhatti M M and Rashidi M M 2017 Numerical simulation of entropy generation on MHD nanofluid towards a stagnation point flow over a stretching surface *International Journal of Applied and Computational Mathematics* **3** 2275–89
[6] Sheikholeslami M 2018 Application of Darcy law for nanofluid flow in a porous cavity under the impact of Lorentz forces *J. Mol. Liq.* **266** 495–503
[7] Nadeem S, Ahmad S and Muhammad N 2018 Computational study of Falkner-Skan problem for a static and moving wedge *Sensors Actuators B* **263** 69–76
[8] Parmar A and Jain S 2018 MHD Powel-Eyring fluid with non-linear radiation and variable conductivity over a permeable cylinder *Int. J. Heat Technol.* **36** 56–64
[9] Khan A U, Hussain S T and Nadeem S 2019 Existence and stability of heat and fluid flow in the presence of nanoparticles along a curved surface by mean of dual nature solution *Appl. Math. Comput.* **353** 66–81
[10] Sheikholeslami M and Seyednezhad M 2018 Simulation of nanofluid flow and natural convection in a porous media under the influence of electric field using CVFEM *Int. J. Heat Mass Transfer* **120** 772–81
[11] Rashidi S, Eskandarian M, Mahian O and Poncet S 2018 Combination of nanofluid and inserts for heat transfer enhancement *J. Therm. Anal. Calorim.* **135** 437–60
[12] Hady F M, Ibrahim F S, Abdel-Gaied S M and Eid M R 2012 Radiation effect on viscous flow of a nanofluid and heat transfer over a nonlinearly stretching sheet *Nanoscale Res. Lett.* **7** 229
[13] Eid M R and Mahny K L 2017 Unsteady MHD heat and mass transfer of a non-newtonian nanofluid flow of a two-phase model over a permeable stretching wall with heat generation/absorption *Adv. Powder Technol.* **28** 3063–73
[14] Al-Hossainy A F, Eid M R and Zoromba M S 2019 SQLM for external yield stress effect on 3D MHD nanofluid flow in a porous medium *Phys. Scr.* **94**
[15] Sheikholeslami M, Li Z and Shafee A 2018 Lorentz forces effect on NEPCM heat transfer during solidification in a porous energy storage system *Int. J. Heat Mass Transfer* **127** 665–74
[16] Khan I, Kahn M, Malik M Y and Salahuddin T 2017 Mixed convection flow of Eyring-Powell nanofluid over a cone and plate with chemical reactive species *Results in Physics* **7** 3716–22
[17] Sadiq M A, Khan A U, Saleem S and Nadeem S 2019 Numerical simulation of oscillatory oblique stagnation point flow of a magneto micropolar nanofluid *RSC Adv.* **9** 4751–64
[18] Nadeem S, Khan A U and Saleem S 2016 A comparative analysis on different nanofluid models for the oscillatory stagnation point flow *The European Physical Journal Plus* **131** 261
[19] Rehman A, Farooq G, Ahmed I, Naseer M and Zulfiqar M 2015 Boundary layer stagnation-point flow of second grade fluid over an exponentially stretching sheet *American Journal of Applied Mathematics and Statistics* **6** 211–9
[20] Ramzan M, Farooq M, Alsaeedi A and Cao J 2015 MHD stagnation point flow by a permeable stretching cylinder with Soret-Dufour effects *Journal of Central South University* **22** 707–16
[21] Rehman A, Nadeem S and Malik M Y 2013 Stagnation flow of couple stress nanofluid over an exponentially stretching sheet through a porous medium *Journal of Power Technologies* **93** 122–32
[22] Pal D, Mal G and Vajravalu K 2015 Mixed convection stagnation-point flow of nanofluids over a stretching/shrinking sheet in a porous medium with internal heat generation/absorption *Communications in Numerical Analysis* **2015** 30–50
[23] Mehmood R, Rana S, Akbar N S and Nadeem S 2018 Non-aligned stagnation point flow of radiating Casson fluid over a stretching surface *Alexandria Engineering Journal* **57** 939–46
[24] Naseem A, Shafiq A, Zhao L and Farooq M U 2018 Analytical investigation of third grade nanofluidic flow over a riga plate using Cattaneo-Christov model *Results in Physics* **9** 961–9
[25] Ghadikolaei S S, Hosseinzadeh K, Ganji D D and Jafari B 2018 Nonlinear thermal radiation effect on magneto Casson nanofluid flow with Joule heating effect over an inclined porous stretching sheet *Case Studies in Thermal Engineering* **12** 176–87
[26] Eid M R 2017 Time-dependent flow of water-NPs over a stretching sheet in a saturated porous medium in the stagnation-point region in the presence of chemical reaction *Journal of Nanofluids* **6** 550–7
[27] Abdelsalam S, Bhatti M M, Zeeshan A, Riaz A and Beg O A 2019 Metachronal propulsion of a magnetized particle-fluid suspension in a ciliated channel with heat and mass transfer *Phys. Scr.* **94**
[28] Hamid M, Usman M, Khan Z H, Ahmad R and Wang W 2019 Dual solutions and stability analysis of flow and heat transfer of Casson fluid over a stretching sheet *Phys. Lett. A* **383** 2400–8
[29] Mackolil J and Mahanthesh B 2019 Exact and statistical computations of radiated flow of Nano and Casson fluids under heat and mass flux conditions *Journal of Computational Design and Engineering.* **6** 593–605
[30] Liu C, Zheng L, Lin P, Pan M and Liu F 2019 Anomalous diffusion in rotating Casson fluid through a porous medium *Physica A* **528** 121431
[31] Aghighi M S, Ammar A, Metivier C and Gharagozlu M 2018 Rayleigh-Bénard convection of Casson fluids *Int. J. Therm. Sci.* **127** 79–90
[32] Nawaz M, Naz R and Awais M 2018 Magnetohydrodynamic axisymmetric flow of Casson fluid with variable thermal conductivity and free stream *Alexandria Engineering Journal* **57** 2043–50
[33] Javed M F, Khan M I, Khan N B, Muhammad R, Rehman M U, Khan S W and Khan T A 2018 Axisymmetric flow of Casson fluid by a swirling cylinder *Results in Physics* **9** 1250–5
[34] Kumar M S, Sandeep N, Kumar B R and Saleem S 2018 A comparative study of chemically reacting 2D flow of Casson and Maxwell fluids *Alexandria Engineering Journal* **57** 2027–34

[35] Ellahi R, Zeeshan A, Hussain F and Abbas T 2019 Two-phase couette flow of couple stress fluid with temperature dependent viscosity thermally affected by magnetized moving surface *Symmetry* **11** 647
[36] Bhatti M M, Zeeshan A, Ellahi R, Bég O A and Kadir A 2019 Effects of coagulation on the two-phase peristaltic pumping of magnetized Prandtl biofluid through an endoscopic annular geometry containing a porous medium *Chin. J. Phys.* **58** 222–34
[37] Majeed A, Zeeshan A, Mahmood T, Rahman S U and Khan I 2019 Impact of magnetic field and second-order slip flow of casson liquid with heat transfer subject to suction/injection and convective boundary condition *Journal of Magnetics* **24** 81–9
[38] Javed T, Ali N, Abbas Z and Sajid M 2013 Flow of an Eyring-Powel non-Newtonian fluid over a stretching sheet *Chem. Eng. Commun.* **200** 327–36
[39] Hayat T, Awais M and Asghar S 2013 Radiation effects in a three-dimensional flow of MHD Eyring-Powel fluid *Journal of the Egyptian Mathematical Society* **21** 327–36
[40] Reddy S R R, Reddy P B A and Bhattacharyya K 2019 Effect of nonlinear thermal radiation on 3D magneto slip flow of Eyring-Powell nanofluid flow over a slendering sheet with binary chemical reaction and Arrhenius activation energy *Advance Powder Technology* **30** 3203–13
[41] Nadeem S and Rehman A 2013 Axisymmetric stagnation flow of a nanofluid in a moving cylinder *Comput. Math. Model.* **24** 293–306
[42] Akbar N , S, Ebaid A and Khan Z , H 2015 Numerical analysis of magnetic field effects on Eyring-Powell fluid flow towards a stretching sheet *Journal of Magnetism Magnetic Materials* **382** 355–8
[43] Vajravelu K, Prasadand K V and Santhi S R 2012 Axisymmetric MHD flow and heat transfer at a non-isothermal stretching cylinder in the presence of heat generation or absorption *Appl. Math. Comput.* **219** 3993–4005
[44] Ellahi R, Sultan A Z, Basit A and Majeed A 2018 Effects of MHD and slip on heat transfer boundary layer flow over a moving plate based on specific entropy generation *Journal of Taibah University for Science* **12** 476–82
[45] Rehman F, Nadeem S and Rizwan U H 2018 Thermophysical analysis of three-dimensional MHD stagnation-point flow of nano-material influenced by an exponential stretching surface *Results in Physics* **8** 316–23
[46] Rehman A, Sallahuddin A, Nadeem S and Iqbal S 2016 Stagnation point flow of Eyring-Powel fluid in a vertical cylinder with heat transfer *Journal of Power Technologies* **96** 57–62
[47] Eid M R 2016 Chemical reaction effect on MHD boundary-layer flow of two-phase nanofluid model over an exponentially stretching sheet with a heat generation *J. Mol. Liq.* **220** 718–25
[48] Lakshmi B K, Sugunmama V and Ramana Reddy V J 2018 Effect of soret and dufour numbers on chemically reacting powell-eyring fluid flow over an exponentially stretching sheet *Journal of Engineering Research and Application* 61–72
[49] Nadeem S, Rehman A and Ali M E 2012 The boundary layer flow and heat transfer of a nanofluid over a vertical slender-cylinder *Journal of Nanoengineering and Nanosystems* **226** 1740349912453806